

See discussions, stats, and author profiles for this publication at: <https://www.researchgate.net/publication/230996181>

Review of FIB-tomography

Chapter · January 2012

CITATIONS

28

READS

1,164

2 authors:



Lorenz Holzer

Zurich University of Applied Sciences

112 PUBLICATIONS 2,268 CITATIONS

[SEE PROFILE](#)



Marco Cantoni

École Polytechnique Fédérale de Lausanne

122 PUBLICATIONS 3,023 CITATIONS

[SEE PROFILE](#)

C H A P T E R 1 1

REVIEW OF FIB TOMOGRAPHY

Lorenz Holzer and Marco Cantoni

1 INTRODUCTION

Over the last few years, FIB tomography has rapidly evolved from a specialized method that was initially used only in a few specialized laboratories, to a common microscopy technique which is nowadays applied in numerous disciplines of materials and life sciences. This successful evolution of FIB-tomography was accompanied by significant improvements of imaging resolution, machine stability, and introduction of user-friendly automation procedures. Due to the combination with a variety of detection modes (low kV BSE, EDX, EBSD, SIMS), FIB tomography has become a versatile method that is now an integral part of the standard equipment of commercially available FIB/SEM machines.

In comparison to other 3D-microscopy techniques, FIB tomography is currently occupying a niche with respect to its resolution and to the volume of the material that can be analyzed (see Figure 11.1; also compare discussion in Mobus and Inkson, 2007). The typical resolutions (i.e., voxel sizes) that can be reached are in the range of tens of nm down to 5 nm. The resolution of FIB tomography is thus clearly better than that provided by X-ray tomography or by the other serial sectioning techniques. Yet even higher resolutions can be achieved with electron tomography by TEM and with atom probe tomography. However, these high resolution 3D-techniques suffer from the drawback of a much smaller sample volume that can be analyzed.

A general problem in quantitative 3D microscopy is representativity. This problem is caused by the limited volume of the analyzed materials. Therefore, resolution and image window size (i.e., volume) must be adjusted according to the feature sizes of interest. For a representative 3D analysis from samples with a wide particle size distribution, a large volume (e.g., cube edge length of 50 μm) and a high resolution (e.g., 10 nm) are required at the

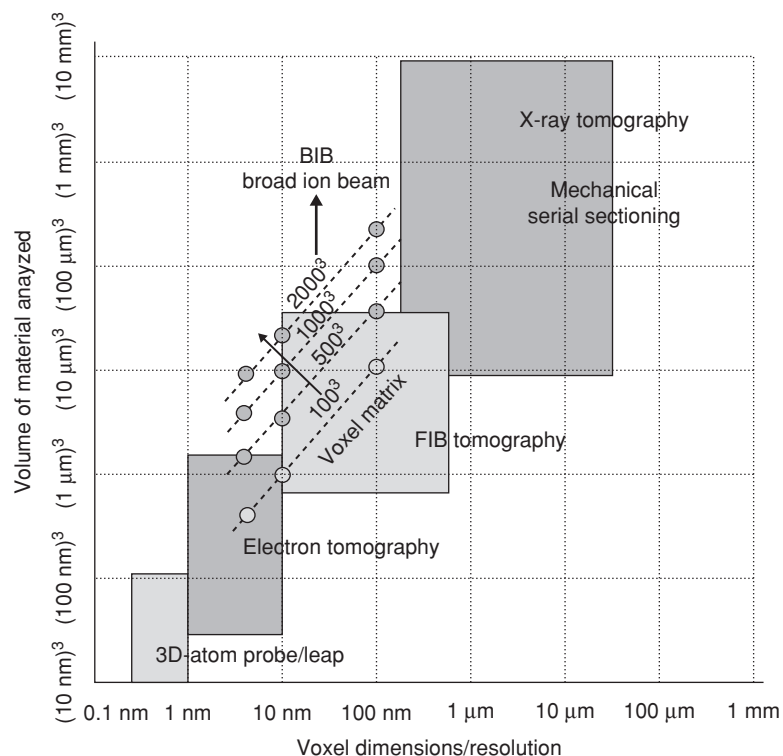


FIGURE 11.1: Comparison of FIB-tomography with other 3D-microscopy methods (modified after Uchic et al., 2007). As illustrated, FIB-tomography is evolving toward larger volumes at higher resolutions, which require a larger voxel matrix.

same time. However, these are contradicting requirements, since the voxel matrix of all 3D techniques is limited by detector capacities and reasonable acquisition time (typically 1000^3 voxels).

Figure 11.2 represents an illustration of the range of cube sizes that can typically be produced with FIB tomography at different resolutions. The particle size distribution of the cement powder under investigation was too wide for a single representative analysis with FIB tomography. Therefore, the powder was separated into five different grain size fractions with average particle diameters (D_{50}) ranging from 0.6 to 14.2 μm . The resolutions were then optimized between 12 to 116 nm for representative analyses, which resulted in cube sizes with edge lengths between 5 and 65 μm . Each cube contains between 1,000 to 4,000 particles, which is the basis for statistical size and 3D shape analysis (Holzer et al., 2006c). It is important to note that the number of images in these analyses was limited to 200–300 images.

In the meantime, the number of images that can be acquired by FIB serial sectioning has significantly increased. Superstacks with 1,000 to 2,000 images (each image with 2048×1536 pixels) can be produced nowadays at a rate of 40 to 60 slices per hour (Cantoni, 2009). Thus, FIB tomography has now reached almost the same resolution as electron tomography (i.e., 5 nm), but with the advantage that it can be applied to much larger sample volumes. Hence, with the current state of FIB tomography, large cubes with a matrix of up to $2,000^3$ voxels can be produced. When imaging with a voxel resolution of 20 nm, this matrix will correspond to a

AU: Is the astreik used here and throughout the text ok?

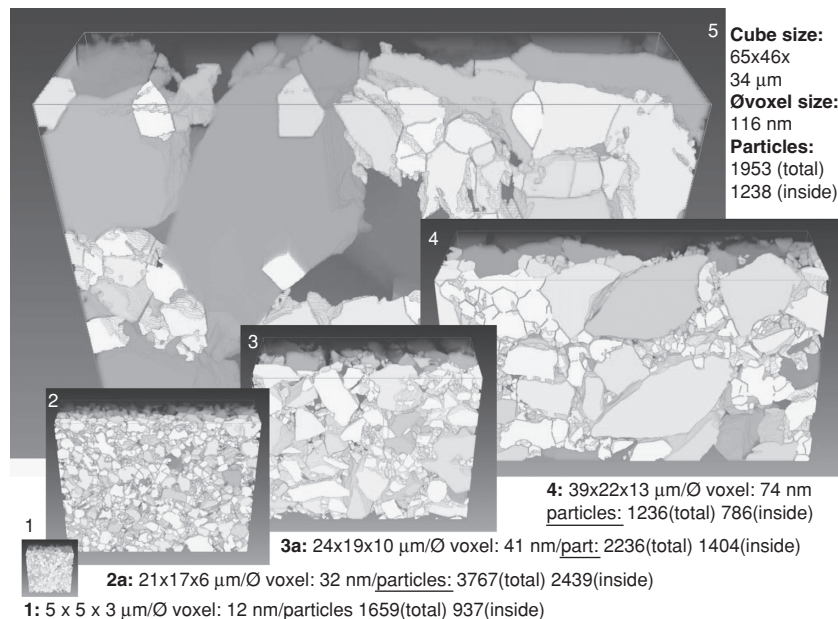


FIGURE 11.2: 3D-analysis of five grain size fractions from ordinary portland cement, adapted from Holzer et al. (2006c). For representative analysis, resolution and volume have to be adapted according to the average grain sizes (D_{50}), which are ranging from 0.6 to 14.2 μm .

cube with edge length of 40 μm . Such a volume would be sufficiently large for the representative analysis of samples with a relatively wide size distribution, which could include all five particle size fractions from Figure 11.2.

Modern FIB tomography thus enables the acquisition of microstructural (BSE), chemical (EDX), and crystallographic (EBSD) 3D-information at resolutions of 5 nm– \times 100 nm, but for sample volumes with an edge length of \times 10 μm . (Note that resolutions are lower for EDX and EBSD). These unique capabilities for 3D imaging with FIB are currently used in a variety of applications, such as:

- Subsurface analysis for diagnostics and failure analysis of semiconductors;
- Investigations of deformation patterns in nanolayered materials;
- Study of the permeability in porous building materials or in oil reservoir rocks;
- Mapping of crystallographic grain orientation in alloys;
- Quantification of triple phase boundaries and percolation in fuel cell electrodes;
- 3D-connectivity of neurons and synapses in brain tissue.

In summary, FIB tomography is still a relatively young microscopy technique. But due to the broad applicability it is spreading rapidly. In this chapter we intend to give a short introduction to the FIB-tomography technique and an overview of the current applications. In the next section, basic aspects of the FIB serial sectioning technique are discussed. These aspects should be taken into account for successful 3D imaging with FIB. In the subsequent section, the succession of methodological innovation steps that led to the current state of FIB tomography is summarized chronologically. Since these innovations opened new possibilities, the present review also includes an overview of the emerging application fields of materials

and life sciences. Finally, in the last section, we briefly discuss the current limitations of FIB tomography and try to formulate the corresponding needs for further developments.

2 FIB SERIAL SECTIONING PROCEDURE

Modern FIB/SEM machines are equipped with both, ion and electron optical columns, which make them perfect tools for serial sectioning at high resolution (see Figure 11.3).

Serial sectioning is an alternating process of sectioning and imaging. Thereby the ion beam (y -direction) is used for sequential erosion of thin layers in the 10 nm range. The sample is placed at the eucentric height, so that the imaging plane (x - y -directions) can be scanned with the electron beam under an angle of 52° without changing sample position. During the acquisition of the image stack, the imaging plane is moving step by step in z -direction due to the sequential ion-milling. The entire serial sectioning procedure includes three phases that are described below: (1) cube preparation and optimization of parameters, (2) serial sectioning, and (3) data processing.

2.1 CUBE PREPARATION AND OPTIMIZATION OF SERIAL SECTIONING PARAMETERS

Before starting the FIB serial sectioning experiment, several imaging and sectioning parameters that are dependent on each other have to be optimized. As discussed in the introduction to

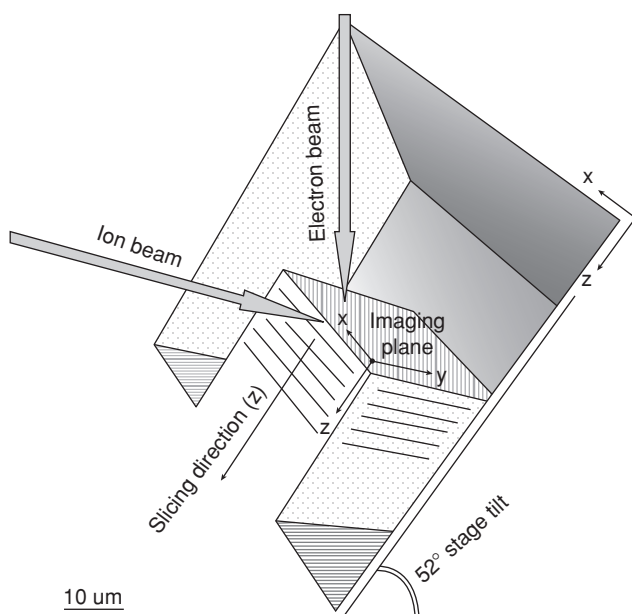


FIGURE 11.3: Illustration of the sample cube geometry, optimized for FIB serial sectioning with a dual beam FIB/SEM machine (modified after Holzer et al., 2004).

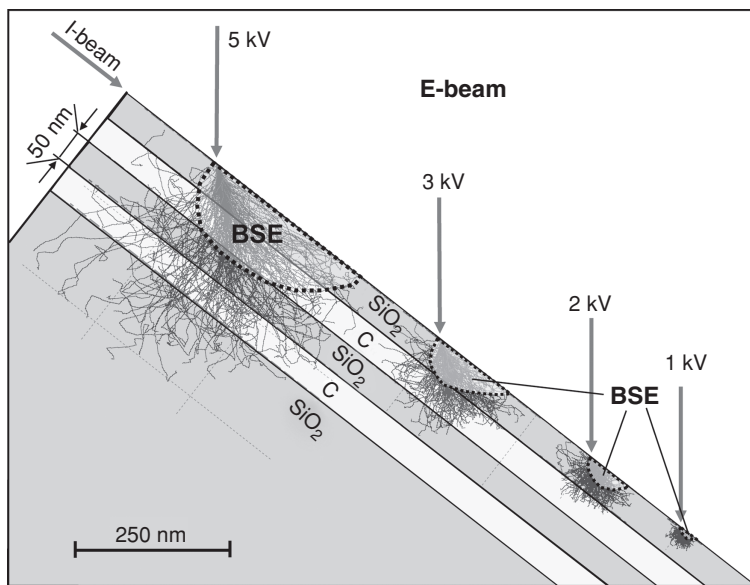


FIGURE 11.4: Electron trajectories in a virtual multilayered material, based on a simulation with Casino-software (<http://www.gel.usherbrooke.ca/casino/What.html>). Note that the size of the interaction volume is strongly depending on the accelerating voltage and that its shape is asymmetrical due to the oblique incident angle in FIB/SEM.

this chapter, resolution and volume of analysis have to be chosen according to the size of the microstructural features in the sample. For the definition of an optimum magnification, the relationship between depth penetration of the electron beam and excitation volume of BSE and X-rays also must be taken into account. This relationship is illustrated in Figure 11.4 for a multilayer carbon-SiO₂ structure. At 5 kV the depth penetration of the electrons is 300 nm, and thus the electron beam protrudes the entire layered structure. In addition, the oblique angle of the incident electron beam also leads to an asymmetrical shape of the interaction volume. The excitation volume for backscattered electrons (indicated by the semitransparent white overlay) is much smaller than the total interaction volume.

Depending on the accelerating voltage, the size of the BSE interaction volume can put drastic limitations to the effective resolution of FIB tomography. In our example (Figure 11.4), the depth of the BSE excitation volume at 5 kV is still larger than 100 nm, which is too large for the investigation of samples with 50 nm layers. In contrast, at 1 kV the BSE excitation volume and the corresponding spatial resolution are in the range of a few nm. For high resolution FIB tomography the ability of low kV imaging thus becomes crucial. The critical aspect for imaging at such low acceleration voltages is then whether the sample and the BSE detector can provide sufficient material contrast. In this context, the latest generation of sensitive BSE detectors, which are optimized for low kV imaging, open new possibilities for 3D imaging at resolutions in the 10 nm range (see, for example, De Winter et al., 2009). Of course, the relationship between depth penetration and accelerating voltage also has to be taken into account for the optimization of the serial sectioning step size. For example, serial sectioning at ≥ 5 kV (SEM) with a step size in the 10 nm range will lead to a strong oversampling without improving the information density of the acquired data volume.

After defining the optimum parameters for serial sectioning, a cube of appropriate size has to be prepared by using the FIB milling capabilities at high beam currents (e.g., 10 nA). About 10 µm wide trenches are milled around the cube in order to enable access of the electron beam to the imaging plane and to reduce shadowing effects in the lower part of the images. The typical cube geometry is shown in Figure 11.3. For serial sectioning in combination with EDX- or with EBSD-detection, this cube preparation is not sufficient and more rigorous preparations techniques such as block lift-out (Schaffer and Wagner, 2008) or milling of a cantilever-shape (Uchic et al., 2006) have been proposed. For the last step of cube preparation, a Pt-layer of approximately 1 µm thickness is produced with *in situ* I-beam deposition in order to protect the cube surface during serial sectioning. In addition, for non-conductive samples a thick metal-coating also should be sputtered (*ex situ*) in order to suppress eventual charging effects. After cube preparation, the sample is ready for serial sectioning.

2.2 SERIAL SECTIONING

The aim of serial sectioning is to produce a regular stack of images, which can directly be transformed into a voxel-based data volume. For this purpose, the thickness of eroded layers should have similar dimensions to the pixel resolution in the imaging plane (i.e., approximately 10 nm). Therefore, the stepwise erosion should be repeated with high precision at a constant z-step size. Because the acquisition of hundreds of images lasts for 20 hours or even longer, drift can become significant. Without correction, the drift in z-direction causes distortions in the reconstructed 3D-microstructure. In contrast, drift components in x- and y-directions are automatically compensated during the off-line data processing with image alignment.

For high resolution FIB tomography an automated serial sectioning with integrated drift correction was introduced (Holzer et al., 2004). However, drift compensation by pattern recognition is affected by continuous degradation of the reference marks during imaging of the x-z-surface with ion-induced secondary electrons (ISE). Hence, the precision of the automated drift correction is decreasing continuously during the sectioning procedure. Fortunately, modern FIB/SEM systems have become much more stable, and usually after a period of stabilization and thermal equilibration drift becomes very small or even negligible. Due to the improved stability in modern FIBs, serial sectioning can be performed without drift correction. Remaining z-drift components can be measured for image sequences of 10, 50, or 100 images and then be compensated linearly during 3D reconstruction. When FIB serial sectioning is combined with EDX, image acquisition takes more time and drift compensation becomes more important. For this purpose an alternative drift correction procedure using electron images at two different magnifications (“overview” and “detail”) was introduced (Schaffer et al., 2007).

In addition to the drift compensation, further correction procedures are needed because of the geometrical peculiarities in dual beam systems: dynamic focus correction is required because of the oblique imaging angle (52°), which also leads to a distortion of x-y-dimensions that have to be corrected accordingly. During the serial sectioning, the imaging plane is shifted in z-direction and therefore focus tracking is required in order to correct for the increasing working distances. When shifting the working distance and imaging under oblique angle, the region of interest is shifted out of the field of view. This has to be compensated with automated region tracking. In modern dual beam FIB/SEM systems, all these phenomena are compensated with the automated sectioning procedure. In this way, image stacks of high quality can be acquired.

2.3 DATA PROCESSING

Extraction of scientifically valuable data from the 3D image volume is a challenging task which is worth paying much attention. Unfortunately, the processing of each material type and each detection mode requires its specific treatment and hence no standard procedures for quantification can be proposed. Nevertheless, the basic procedures of stack processing can be described as follows:

- 3D-reconstruction by stack alignment and image registration;
- Correction of image defects (e.g., noise reduction with gauss-filters);
- Segmentation and recognition of individual objects for subsequent statistical analysis;
- Visualization of voxel-based grey-scale data or surface visualization of segmented features by triangulation;
- Quantitative analysis and statistical measurement of features: e.g., particle/pore size distributions, surface area, triple phase boundary lengths, feature counting, etc.

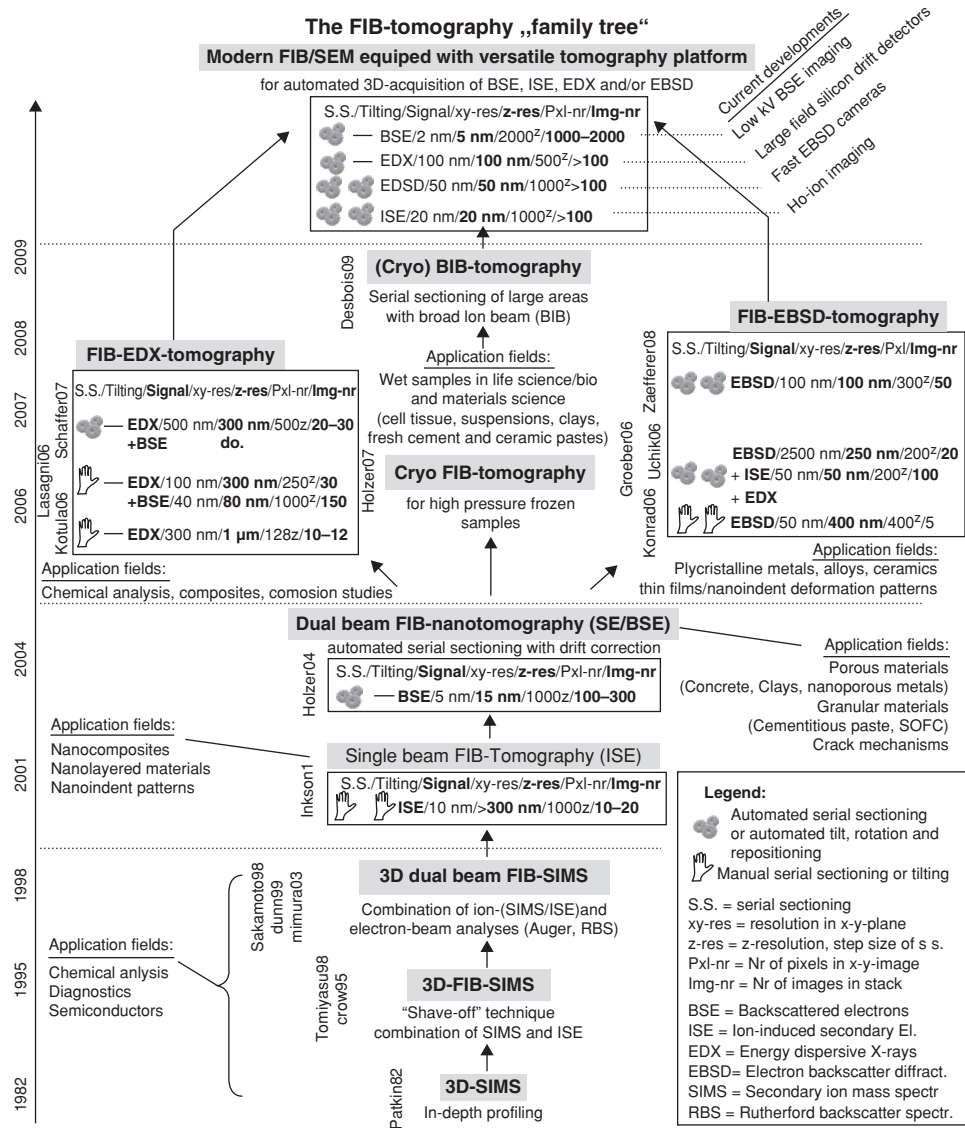
A more detailed description of image analysis principles is given elsewhere (Russ, 1999). Selected examples for quantitative analysis of granular textures and porous networks based on 3D data from FIB are presented in section 3.3.

3 CHRONOLOGICAL EVOLUTION OF FIB TOMOGRAPHY

Today, commercial FIB/SEM machines provide automated and user-friendly solutions for 3D characterization by serial sectioning. This advanced stage of FIB-tomography has evolved over a period of nearly three decades. Initially the FIB machines were not optimized for automated serial sectioning but rather for user-operated cross-sectioning and TEM-lamella preparation. The development of advanced serial sectioning capabilities is based on numerous methodological innovation steps, which typically were initiated in pilot projects of pioneering research labs. In a second step, usually the methodological improvements were automated by means of scripting routines. Finally, when these routines proved to operate successfully for important scientific and technological applications, then they were incorporated into the standard equipment of commercially available FIB machines. The improvements of the FIB serial sectioning also opened new possibilities for 3D microstructure characterization and hence new fields of applications emerged. This evolution, which is illustrated in Figure 11.5, is discussed in the following sections.

3.1 PIONEERING STAGES OF FIBTOMOGRAPHY: SUBSURFACE ANALYSIS WITH 3D-SIMS

Initially, 3D-analysis using a focused ion beam was performed mainly in combination with secondary ion mass spectrometry (SIMS) for subsurface chemical analysis and for diagnostics of artifacts in IC-production. In these fields, 3D analysis with in-depth profiling by SIMS was introduced already in the early 1980s (Patkin and Morrison, 1982) and improved later (e.g., by Hutter and Grasserbauer, 1992). At that time the lateral resolution was typically above the μm -scale. The corresponding depth-resolution was ill defined because of differential sputtering,

**FIGURE 11.5:** Chronological evolution of FIB-tomography and the corresponding application fields.

which occurs during in-depth profiling with the ion beam orientation being perpendicular to the surface (see Figure 11.6, left).

During the 1990s, FIB columns with improved spatial resolution and with higher current densities became available. These improvements enabled the acquisition of sequential SIMS-mappings at sub-μm spatial resolution. Such FIB-SIMS systems were used, e.g., for the localization of contaminating nanoparticles within multilayer IC structures (Sotah et al., 1991) and for analyses of semiconductor materials (Crow et al., 1995). For the correction of the artifacts from depth profiling the so-called “shave-off method” was then introduced (Tomiyasu et al., 1998). In the shave-off technique the sample surface is tilted parallel to the ion beam and the uneven surface layer can be polished by “in-plane” erosion (see Figure 11.6).

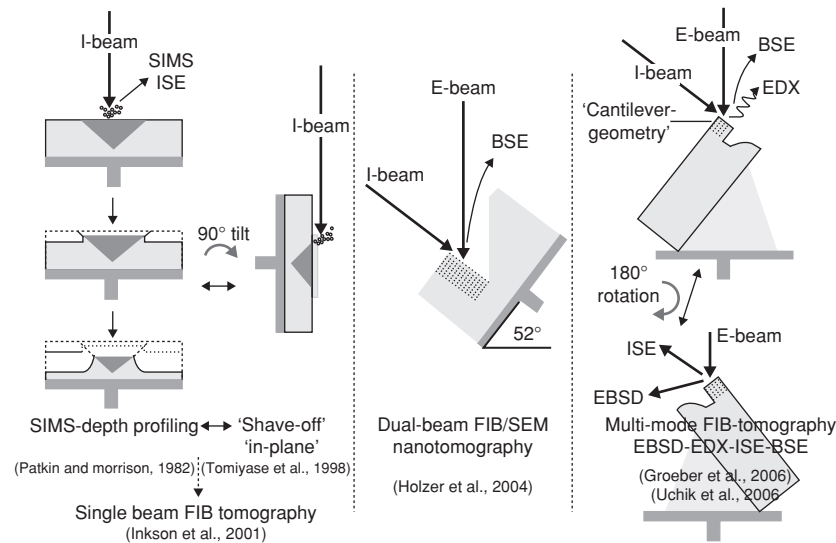


FIGURE 11.6: Geometrical concepts of FIB serial sectioning. Left: SIMS-depth profiling and shave-off for single beam FIB. Middle) FIB-nanotomography with dual beam FIB (no tilting and repositioning necessary). Right: Multimode FIB-tomography for 3D-EBSD and optional combination with ISE, EDX and BSE using cantilever geometry and sample rotation.

The combined procedure of sequential depth profiling and shave-off erosion with single beam FIB-SIMS systems included tilting and repositioning between the alternating steps. Because this procedure is very time consuming, usually small stacks with only 5 to 20 maps were acquired. In addition, mechanical instabilities related to the stage tilting and sample repositioning still imposed limitations to the z-depth resolution, which was typically several hundreds of nm.

The first prototypes of dual beam FIB-SEM systems were then introduced, which enabled efficient 3D acquisition of combined chemical and structural information by using quadrupol SIMS together with secondary electron imaging (Sakamoto et al., 1998) and/or with auger spectroscopy (Dunn and Hull, 1999). Nevertheless, since these systems were mainly dedicated to the detection of secondary ions (SIMS) or ion-induced secondary electrons (ISE), the serial sectioning procedure still required time-consuming tilting and sample repositioning between the alternating “shave-off” and imaging steps, which were both performed with the ion beam at different stage positions.

In the retrospective, 3D-SIMS can be considered as a pioneering sub-discipline of FIB tomography. Numerous technological innovations have been introduced in the field of FIB-SIMS five to ten years earlier than in the more “conventional” field of FIB/SEM-tomography. For example, high resolution SIMS tomography with 20 nm isometric voxels was reported already before the year 2000 (Dunn and Hull, 1999). Alternatively, serial sectioning with a large mapping size in the order of $\times 100 \mu\text{m}^2$ was achieved by combining FIB-SIMS with chemically assisted ion beam etching (Tanaka et al., 2003). Last but not least, 3D-SIMS was often also combined with various other beam techniques such as Auger spectroscopy (Sakamoto et al., 1998) and Rutherford backscattering (Mimura et al., 2003). These combinations provided interesting complementary 3D information for combined microstructure and chemical 3D-characterization. Nevertheless, the early papers about 3D-FIB-SIMS were usually focusing

on specific methodological and analytical details, whereas in-depth investigations of the microstructure-property relationships were missing. For a broader application of the FIB tomography technique in materials science, further improvements of the imaging capabilities and automation of the serial sectioning were required.

3.2 SERIAL SECTIONING WITH SINGLE BEAM FIB: INITIATION OF FIBTOMOGRAPHY *SENSU STRICTO*

The term *FIB tomography* was first used in conjunction with serial sectioning that was performed manually with a single beam FIB (Inkson et al., 2001b). By taking a series of 15 sequential images that were separated by irregular step sizes between 260 and 660 nm, the subsurface nanoindentation deformation of Cu-Al multilayers could be visualized. Thereby the plastic thickening of the Al-layer and its delamination from the Al₂O₃-substrate could be analyzed by so-called displacement maps that were extracted from the corresponding 3D-reconstructions. This single beam FIB-tomography technique was subsequently also applied for 3D grain shape analysis in Fe-Al nanocomposites (Inkson et al., 2001a), for 3D reconstruction of MOSFET gate morphology (Inkson et al., 2003) and for subsurface damage analysis in Al-Al/SiC nanocomposites (Wu et al., 2003).

A major drawback of the single beam FIB tomography was the limitation in z-resolution, related to the manual stage tilting. In fact, special 3D reconstruction techniques were required for the z-correlation of specific objects that could be identified in the single 2D images (x-y-plane). A new technique for shape based interpolation (SBI) was then introduced, which enabled accurate grain shape reconstruction of γ' -phase precipitates in Ni-based superalloys (Kubis et al., 2004). However, 3D analysis of small objects in the sub- μm range was still limited by the relatively large z-spacing in the 100 nm range. Thus, for 3D analysis of nanostructured materials, it was necessary to develop a serial sectioning procedure with repetitive z-step size in the lower nm-range.

3.3 AUTOMATED DUAL BEAM FIB NANOTOMOGRAPHY

With the introduction of dual beam FIB/SEM systems new possibilities for automated serial sectioning arose. In these FIB/SEM systems no tilting is necessary for serial sectioning because the dual beam geometry is optimized for synchronous operation of ion and electron beams under an angle of 52° (see Figure 11.3 and Figure 11.6, middle). Automated serial sectioning without tilting and repositioning enabled the acquisition of larger stacks with hundreds of images at higher precision and in shorter time. By using the machine-related scripting language, a fully automated “FIB nanotomography” procedure was developed for stack acquisition by overnight processing with a repeatable z-step size in the 10 nm range (Holzer et al., 2004). The automated FIB nanotomography procedure included drift correction based on pattern recognition. This drift correction was important because the early dual beam FIB/SEM systems were not yet optimized for long time stability and therefore various sources of electromagnetic and mechanical drift became apparent when sectioning at z-step sizes below 50 nm.

An alternative version of drift-corrected FIB nanotomography was based on shape analysis of reference marks (so-called z-spacer trenches), which were applied before serial sectioning by using the precise FIB milling capabilities (Bansal et al., 2006). Based on the profile shape of the

spacer trenches in the serial images, uneven step sizes could be identified, and this information was then used for drift-corrected 3D reconstruction. However, since this procedure requires time-consuming FIB milling of reference marks, only a limited number of very thin samples ($\times 100$ nm total thickness) were analyzed in this way, e.g., for the study of θ' -precipitates in Al-alloy.

In contrast, the “normal” FIB nanotomography technique was continuously improved over the last few years and is now commercially available, so that it is used in a growing number of investigations (see e.g. Jeanvoine et al., 2006 or McGrouther and Munroe, 2007). The next few subsections of this chapter contain a short summary of FIB tomography applications for the 3D-investigation of cementitious building materials, ceramics, solid oxide fuel cells, and biological tissue.

3.3.1 3D-analysis of porous materials

FIB nanotomography is often used for the quantitative characterization of porous and granular microstructures. In this context it is important to note, that the geometrical concepts for the quantification of porous and granular microstructures are fundamentally different. Granular microstructures are composed of discrete objects, whereas pore structures usually form a continuous network. These contradicting geometrical concepts were mathematically introduced together with a description of algorithms for the quantification of continuous and discrete size distributions (Münch and Holzer, 2008), which were then used in combination with FIB nanotomography for the study of granular and porous microstructures.

In porous materials, permeability and corresponding transport properties are controlled by topological features such as connectivity, (de-)percolation, and dimensions of the pore necks. Quantification of these features can only be performed on the basis of suitable 3D-images. Thereby, FIB nanotomography opens new possibilities for analysis of pore structures with dimensions on the sub- μm scale, which was demonstrated for ceramic BaTiO_3 (Holzer et al., 2004), for hydrated cement (Holzer et al., 2006a; Holzer et al., 2006b; Münch et al., 2006b; Münch and Holzer, 2008; Trtik et al., 2008), for clay-rich materials and porous rocks (Desbois et al., 2008; Desbois et al., 2009; Holzer et al., 2010) and for crack growth in metals (Holzapfel et al., 2007).

An example of a quantitative pore structure analysis based on FIB tomography is illustrated in Figure 11.7 for hydrated cement paste (Holzer et al., 2006a). Thereby, the results from 3D analysis and from mercury intrusion porosimetry give significantly different pore size distributions (PSD). The PSD curve of mercury porosimetry has a discontinuous shape, whereas the PSD curves based on 3D analysis are nearly linear (Figure 11.7, bottom left). The same pattern with systematically different results from 3D-FIB and from mercury porosimetry was observed in other porosity investigations (compare Münch and Holzer, 2008). This different behavior is explained by the ink-bottle effect in mercury porosimetry, which leads to an overestimation of the smaller pores with sizes close to the so-called breakthrough diameter. Hence, more reliable size distributions are obtained from 3D microscopy, which is not affected by the ink-bottle effect. In addition, not only the bulk porosity can be characterized with tomography. By careful analysis of the 3D-images, the total porosity in cement paste (Figure 11.7, top left) can be subdivided into two different types of pores. The so-called “internal” porosity is hosted inside the hydrated cement grains (Figure 11.7, middle left, dark gray regions), whereas the “matrix” porosity is hosted in the interstitial region between the hydrated cement grains. The connectivity between the two types of pores can be characterized based on the analysis of the skeletonised 3D-pore network (top right). Thereby, the connections

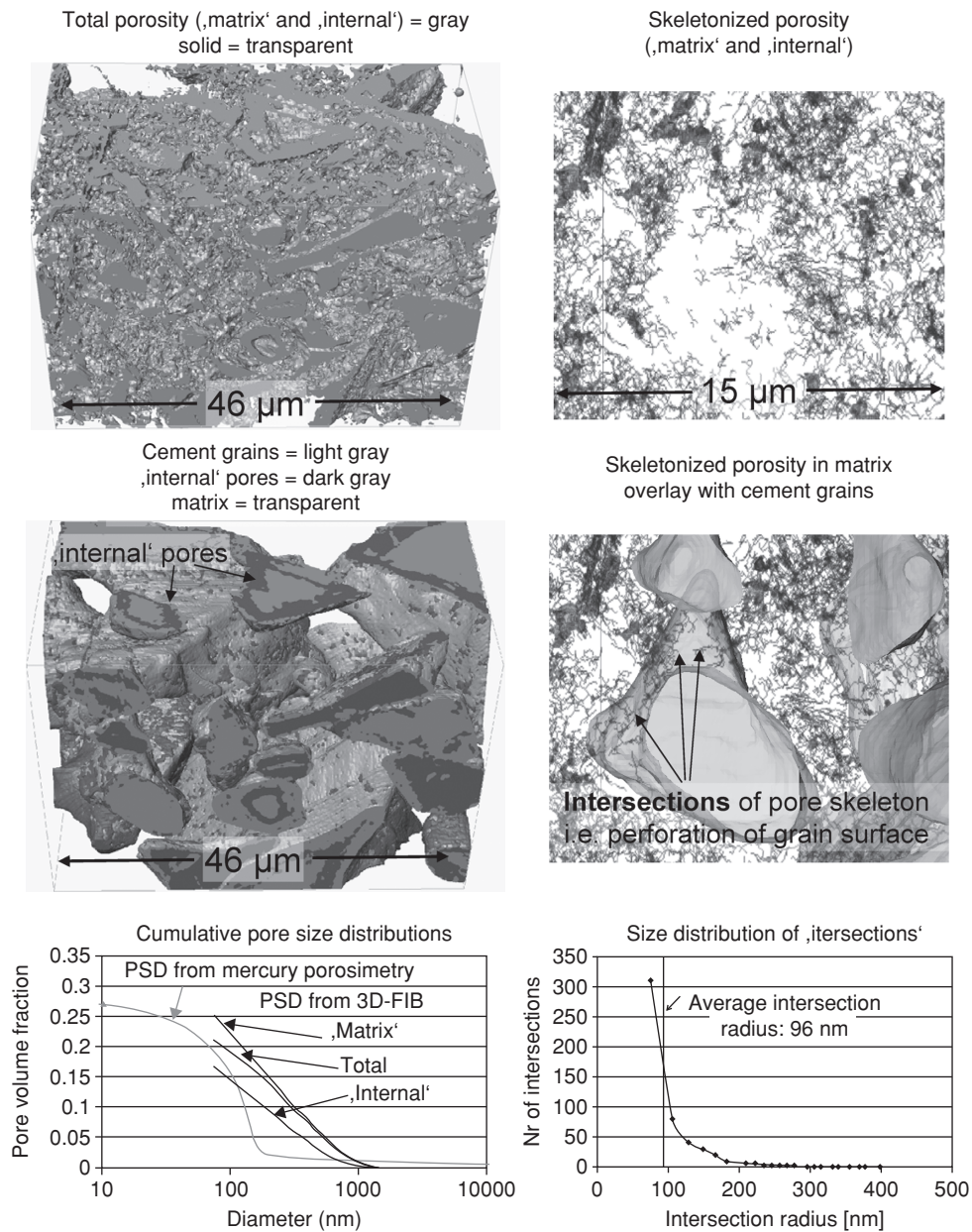


FIGURE 11.7: 3D-analysis of porosity in hydrated cement paste (modified after Holzer et al., 2006a). 3D images allow the distinction of “matrix” and “internal” pore types. The connectivity between the two pore types is quantified by statistical analysis of the intersections where the pore network is perforating the particle surfaces.

between the “internal” and the “matrix” porosity are represented by the intersections of the pore skeleton through the particle surfaces (middle right). A statistical description of the intersections (i.e., size distributions and number of intersections per surface area) can be extracted from the skeletonized pore structure (Figure 11.7, bottom right). Since this information is crucial for the understanding of transport and associated degradation processes, this kind of information should be incorporated in future computational models on concrete and cement permeability and degradation.

3.3.2 3D-analysis of granular materials

In granular materials, not only the particle size distributions but also the particle shape and parameters related to the particle packing (i.e., coordination numbers, particle-particle interfaces) are relevant for the understanding of mechanical properties (strength, elasticity) and flow behavior (rheology). These parameters are specific aspects of the 3D microstructure. Before such complex topological parameters can be extracted from tomography data, the individual particles have to be identified reliably. Unfortunately, recognition of discrete objects (i.e., individual particles) in the images from FIB tomography represents a major challenge, because BSE contrast usually does not reveal the grain boundaries in polycrystalline materials. Therefore, specific computational methods have been introduced for object recognition in densely packed granular materials (based on “splitting”), together with stereological procedures for the correction of boundary truncation effects (Münch et al., 2006a). An example of the object recognition by particle splitting is illustrated in Figure 11.8 (see also Figure 11.2).

FIB nanotomography in combination with accurate object recognition was then used for quantitative studies of particle size distributions and surface area fractions in densely packed cement powder (Figure 11.9). Also more complex parameters such as particle shape and particle-particle contacts were elaborated with FIB nanotomography (Holzer et al., 2006c; Holzer et al., 2007; Zingg et al., 2008; Holzer and Münch, 2009). From the particle shape

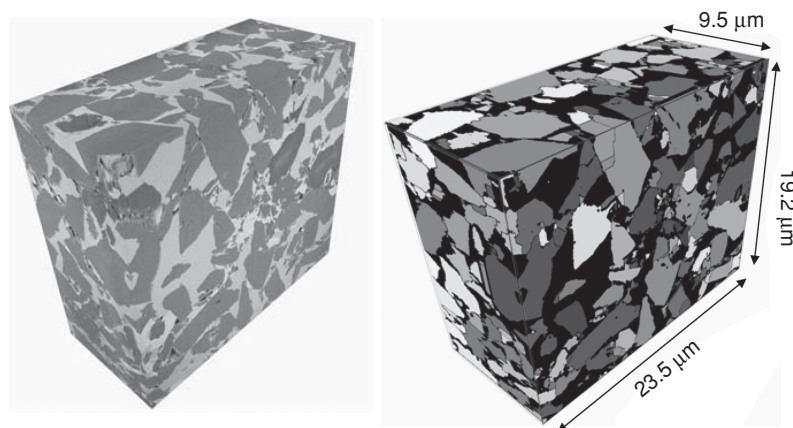


FIGURE 11.8: Granular texture of densely packed cement powder (modified after Holzer and Münch, 2009). Left: 3D-reconstruction from original FIB/SEM gray scale images. Note the poor contrast between the cement particles. Right: Object recognition by splitting. Individual particles are labelled with different colours (Münch et al., 2006a).

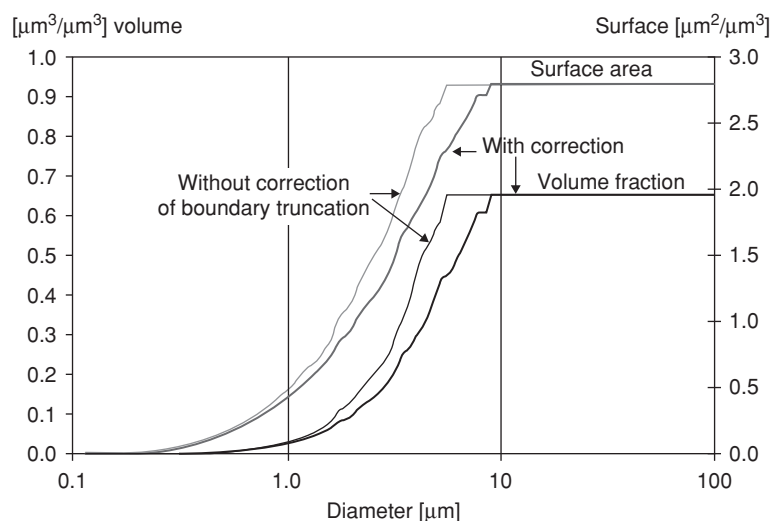


FIGURE 11.9: Quantification of particle size distributions related to cumulative volume fraction (black) and cumulative surface area (gray) of the cement sample shown in Figure 11.8 (modified after Holzer and Münch, 2009).

analysis, unique description of inertia axes for different particle size classes could be obtained. This information was then used as input for simulations of granular flow in cementitious suspensions by means of dissipative particle dynamics (Martys, 2005). Furthermore, in metallurgical applications FIB nanotomography was also used to classify complex graphite morphologies in steel (Velichko et al., 2008).

3.3.3 3D analysis of electrodes in solid oxide fuel cells (SOFC)

Solid oxide fuel cells (SOFC) efficiently convert chemical energy into electrical power. The performance of the fuel cells is strongly related to the microstructure of the porous electrodes. Thereby, 3D connectivity of the pore network is controlling transport of fuel and air, whereas ionic and electronic currents are conducted by the percolating metal- and ceramic-phases (McLachlan et al., 1990). The electrochemical charge transfer reactions take place at the triple phase boundaries. Also, catalytic activity of pore-solid interfaces and associated surface area are important. Thus, the electrode performances are strongly dependent on 3D microstructural parameters, which can only be determined based on high-resolution tomography. In this context, the recent improvements of FIB tomography enable the collection of unique topological information that gives new insight into the complex microstructure-property relationships of SOFC electrodes. Consequently, numerous research institutes have started to use FIB nanotomography for fuel cell investigations (Boukamp, 2006; Wilson et al., 2006; Gostovic et al., 2007; Izzo et al., 2008; Wilson et al., 2009a; Wilson et al., 2009b; Smith et al., 2009; Gostovic et al., 2011; Holzer et al., 2011).

An example of a 3D-microstructure analysis from a composite porous SOFC anode is illustrated in Figure 11.10. After segmentation, the three principal components (Ni, CGO, porosity) can be visualized and quantified separately. The skeletonization shows the potential transport paths whereby Ni (for electron conduction) is much coarser than CGO (Ce-Gd-Oxide, ionic conduction) and the pores (transport of fuel). The challenge for future 3D

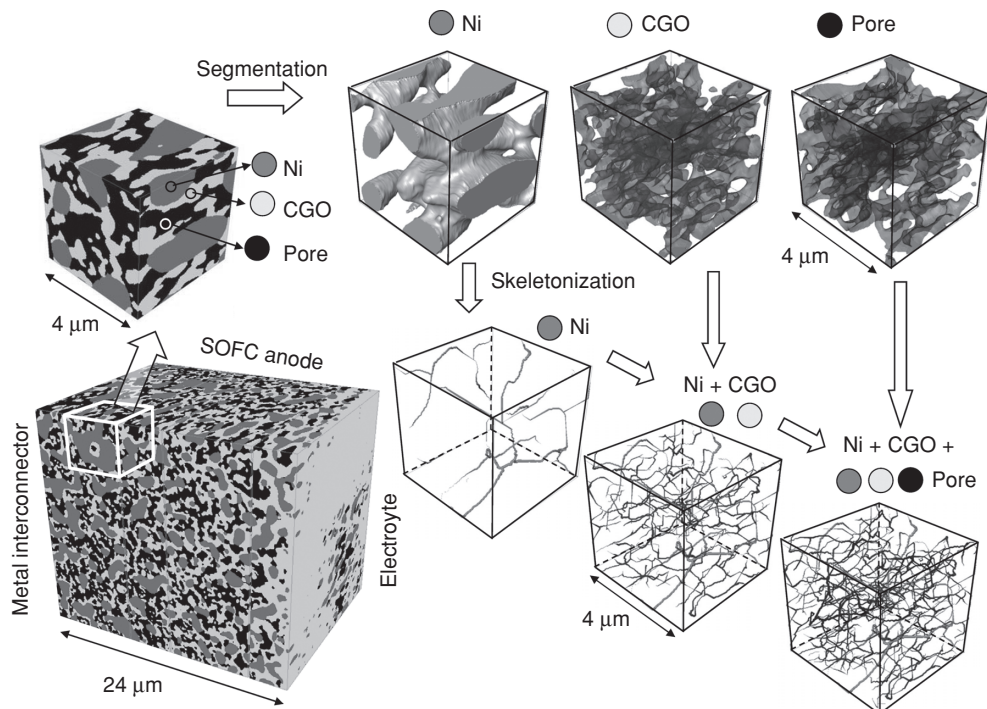


FIGURE 11.10: 3D-microstructure of a composite anode in a solid oxide fuel cell (SOFC) (adapted from Holzer et al., 2011). The segmented Nickel, Ce-Gd-Oxide (CGO), and pore phases are shown for a small subvolume (4 μm edge length). The skeletonised structures illustrate the potential transport pathways for electrons (Ni), oxygen-ions (CGO), and fuel (pore). The skeleton overlay (bottom right) shows the dense intercalation of the three phases and transport pathways.

investigations of fuel cells is to elaborate the way in which the different transport and electrochemical processes are related to the various microstructural parameters and how this knowledge can be used for the improvement of the reaction kinetics and the overall cell performance.

3.3.4 FIB tomography in life science applications

For many years, the exploration of cells and tissues with electron microscopy has been limited to imaging a sample's topography using SEM, and thin section imaging with serial sectioning TEM. Tilt series electron tomography provides high-resolution 3D imaging over a limited volume, but now FIB-SEM tomography has the potential to explore cells and tissue on a much larger scale. The studies so far have mainly been limited to the use of traditional resin embedding approaches in which material has been chemically fixed with aldehydes, heavy metal stained, dehydrated, and resin embedded. These sample blocks are therefore robust and easily manipulated in the FIB/SEM. Imaging the stained cellular material relies therefore on differences in the densities of stained and unstained structures. Backscattered images have so far shown contrast that is comparable to the one from thin sections in the TEM, though at a lesser resolution. However, these are still sufficient for observing all membrane bound structures within different types of cells.

Heymann et al. (2006) used ion beam milling to explore both animal and plant cells. More recently, the same group has shown how this technique is improving rapidly with the ability of seeing the 3D arrangement of cell organelles (Heymann et al., 2009). This higher resolution capability has been used to analyze the inner architecture of chromosomes (Schroeder-Reiter et al., 2009) as well as the connectivity between neurons in the brain (Knott et al., 2008). This latter study has brought the FIB/SEM microscopes to the attention of neuroscientists as synaptic connections are too small to be seen with optical approaches. Until recently the only way of trying to make sense of the highly complex interconnectivity between neurons in the brain was with TEM. Denk and Horstmann (2004) demonstrated how backscattered imaging of a block face can be used to image neural tissue, and today FIB/SEM is drawing increasing interest as a tool for exploring the brain as well as other tissues.

Most of these studies were carried out on conventionally prepared material. Only Heymann et al. (2006) has so far used frozen hydrated samples. In this study, cryo-fixed yeast cells were analyzed by generating images of the membranous structures. This was achieved by carefully allowing the surface of the milled block face to sublime slightly, and the relief of this face being seen with the imaging beam. Again, this method provided clear images of internal membrane structures. However, achieving tomographic image series will require some further developments.

As described earlier in this chapter, “close to surface” information is required for high-resolution serial sectioning. Thereby the interaction volume of the electron beam in the sample is defined by the beam energy and the sample density. An energy-selective backscattered detector (EsB) on the ZEISS NVision40 FIB can be used at low accelerating voltages (below 2kV) and tuned so that backscattered electrons that have lost only a few hundred eVs are detected. In this way the escape depth of the backscattered electrons is below 5nm. This allows for details such as cell membranes to be seen, with a contrast and resolution that are normally only seen with serial sectioning TEM (ssTEM). We have used these capabilities for imaging of mammalian tissue samples as well as cultured cells grown on various artificial substrates. These were prepared using aldehyde fixation and then post fixed and stained with osmium tetroxide and uranyl acetate. The samples were then embedded in Durcupan resin, and once cured, blocks were trimmed with glass knives using an ultramicrotome. The following examples show the clear potential of FIB nanotomography in the “bio-nano” field:

Example A/Bio-compatibility (Figure 11.11) shows a cell grown on ceramic coated steel. 600 slices were milled through resin embedded cell/ceramic layer/steel with 20 nm slice thickness at 10 nm image pixel size. The volume covers $20 \times 15 \times 12 \mu\text{m}$ with a voxel size of $10 \times 10 \times 20 \text{ nm}$. The reconstruction permits the 3D morphological analysis of the cell and its organelles as well as the visualization of the ceramic surface and grain boundaries in the steel substrate below. The inspection of the interface between the cell and the ceramics reveals that in this particular case the cell is only attached at a few spots.

For Example B/Brain tissue of rat hippocampus (Figure 11.12), 1,600 slices of 5nm thickness were cut and imaged in 40 hours by automated acquisition. The image pixel size is 5 nm ($2,048 \times 1,536$ pixels per image). The volume of this stack covers $10 \times 8 \times 8 \mu\text{m}$ with a voxel size of $5 \times 5 \times 5 \text{ nm}$. Cell membranes, vesicles and mitochondria with their internal membranes are perfectly resolved. This allows for the identification of different types of neurons and the synaptic contacts that exist between them. Within this volume there are more than 800 synapses present. Future research activities will focus on the integration of the FIB-3D-information from brain tissue into computational models from neuroinformatics.

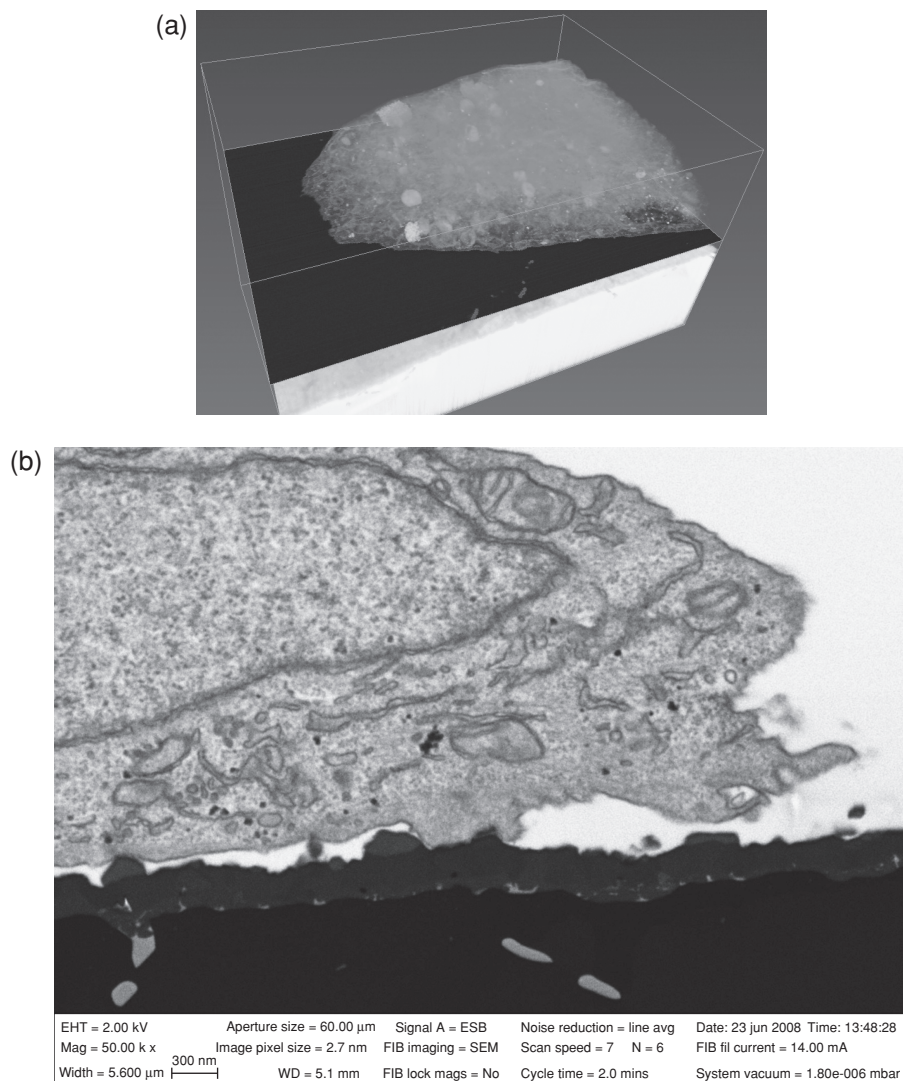


FIGURE 11.11: Bio-compatibility study of cell-substrate interface (a): 3D-reconstructed cell on ceramic coated steel. (b): detailed view of a single SEM image of the FIB-stack. Contrast inverted for better visualization of membrane structures.

3.4 CRYO FIB TOMOGRAPHY AND COMBINATIONS WITH BROAD ION BEAM (BIB)

For the investigation of wet samples, cryo FIB tomography was introduced (Holzer et al., 2007). Thereby, cryo-techniques from life-sciences such as high-pressure freezing, cryo-transfer, and cryo-SEM were combined with FIB serial sectioning. In the first cryo FIB tomography studies, this methodology was used for the quantification of microstructural changes in complex cementitious suspensions. The microstructural changes, including particle-number-densities, surface area, and size distributions, could be correlated with reactions of the early cement hydration (precipitation, agglomeration, dispersion by surfactants) and with the corresponding

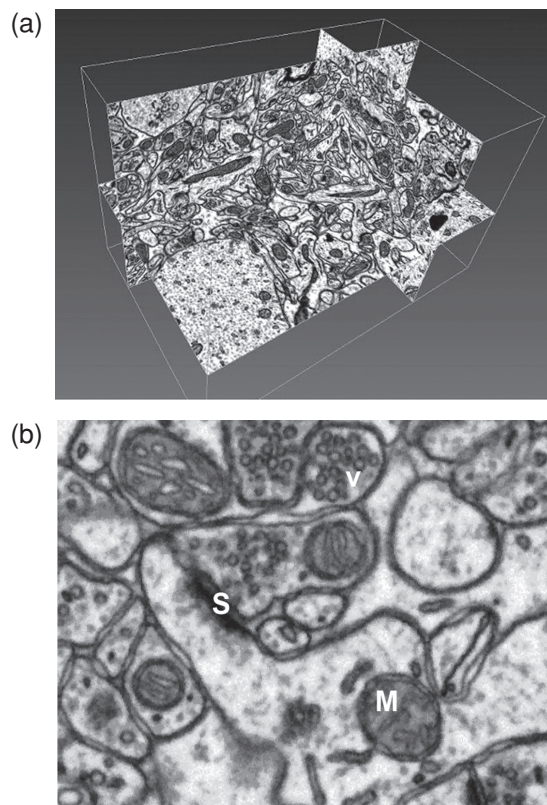


FIGURE 11.12: 3D-investigation of brain tissue (a): orthogonal slices representing a volume of $10 \times 10 \times 8 \mu\text{m}$. (b): detailed view of a $3 \times 2.5 \mu\text{m}$ area inside the FIB-stack which illustrates a synapse (S), vesicles (v) and mitochondria (M).

rheological properties of fresh cement pastes (Holzer et al., 2007; Zingg et al., 2008; Holzer and Münch, 2009).

As mentioned in the introduction, a larger field of view is necessary for representative analysis of heterogeneous samples. This is of particular interest in geological applications of natural rocks (e.g., oil/gas reservoir rocks), which typically have wide pore size distributions that are spanning from nm- to mm-scales. For such investigations the capabilities of cryo-serial sectioning was extended by a combination of SEM with broad ion beam (BIB), which enables 2D-imaging and serial sectioning of larger sample areas (100 nm^2 to mm^2) due to much higher sputter rates (Desbois et al., 2009). Thin layers of $\times 100 \text{ nm}$ thickness can be removed by BIB erosion under a shallow angle. Thereby, deeper levels of the sample are protected with a massive metal blend. The geological applications of cryo-FIB and cryo-BIB include pore studies in gas/oil reservoirs, brine-filled grain boundaries in rock salt (Desbois et al., 2008), engineered bentonite barriers, and porous clay host rocks of radioactive waste repositories (Desbois et al., 2009; Holzer et al., 2010).

The above review of FIB tomography and the corresponding applications in materials, life, geo- and environmental sciences is by far not complete. Further FIB-3D studies were performed for example on the topic of crack formation (Elfallagh and Inkson, 2008; Elfallagh and Inkson, 2009). The large number of applications documents the unique imaging capabilities of the FIB tomography method. However, one of the major restrictions of FIB tomography is given by the relatively low BSE-contrast in polycrystalline ceramics and alloys (see discussion in Cao et al., 2009). Consequently there is a need to combine FIB serial sectioning with alternative

detection modes that deliver additional information on the internal structure such as spatial distribution of chemical elements (EDX) and crystal orientations (EBSD). The combinations of FIB tomography with these detection modes are discussed in the subsequent sections.

3.5 FIB-EDX-TOMOGRAPHY:TOWARD 3D SPECTRAL IMAGING (TSI)

By combining FIB-serial sectioning with EDX-detection, information about the 3D elemental distribution at μm - and sub- μm scales can be acquired. However, for the FIB-EDX tomography some peculiarities that are inherent to the EDX-method have to be taken into account: (a) EDX cannot be performed at low kV, which results in a relatively large excitation volume (see Figure 11.4). Consequently the corresponding spatial resolution is in the range of $\times 100$ nm up to $>1 \mu\text{m}$. (b) Acquisition time with SiLi-detectors is much longer (typically 0.5 up to >1 hour per 2D-mapping). The recent introduction of silicon drift detectors with wide collecting angle enables higher count rates and faster acquisition. (c) Significant charging generally occurs in non-conductive materials due to high accelerating voltage and slow scanning rates. (d) Significant drift components are observed due to long milling time (large z-step-size), the slow EDX-acquisition and the mentioned charging effects. (e) Artificial x-ray counts are produced from scattered electrons which interact with the surrounding walls of the sample.

Due to these problems, automation of FIB-EDX-tomography is more challenging than “normal” FIB-SEM-tomography. Therefore, serial sectioning with EDX was initially performed only manually. In this way the 3D structure of CuAl-alloys and corrosion products in layered CuNiAu samples were investigated (Kotula et al., 2006) by acquisition of 10 to 12 sequential EDX maps. The individual imaging planes were separated by $1 \mu\text{m}$ in z-direction, whereas the pixel resolutions in x-z-directions were 300 to 400nm. Already with the limited manual acquisition, a relatively large amount of chemical data (full spectral information for each voxel in a matrix of $128 \times 128 \times 10$) was generated. For efficient processing and accurate identification of the principal components, computational methods based on multivariate statistical analysis (MSA) were introduced (Kotula et al., 2003; Kotula et al., 2006).

Subsequently an automated serial sectioning procedure was presented which enabled synchronized acquisition of sequential EDX-mappings in combination with SE/BSE-tomography (Schaffer et al., 2007). It turned out that drift correction represents the most challenging problem for 3D-EDX-automation. Due to high ion beam currents which are used for efficient erosion of relatively thick material layers (z-step size: $\times 100$ nm to $1 \mu\text{m}$) drift correction based on reference pattern recognition with ISE imaging was not possible because the reference pattern would be eroded during the analysis. Therefore a post-acquisition drift correction method, which is based on image registration of BSE “overview” and “detail” images, was developed (Schaffer et al., 2007). The automated FIB-EDX-tomography was then successfully applied for the analysis of the 3D microstructures in CaMgTiO_x and in FeAl-alloy (see Figure 11.13). For further improvement of the EDX data quality, the small cube of analysis was transferred to a TEM-holder by using the block lift-out technique (Schaffer and Wagner, 2008). In this way artificial X-ray signal from the surrounding sample walls and shadowing effects can be suppressed.

Combined FIB-SEM-EDX-tomography was then also used for the characterization of eutectic microstructures in AlSi-alloys (Lasagni et al., 2006; Lasagni et al., 2007; Lasagni et al., 2008a). Due to the combination of BSE images (z-resolution 50 nm) with EDX mappings (z-resolution 500 nm, but with better contrast), complementary information could be acquired, which improved segmentation and recognition of minor components that were otherwise not

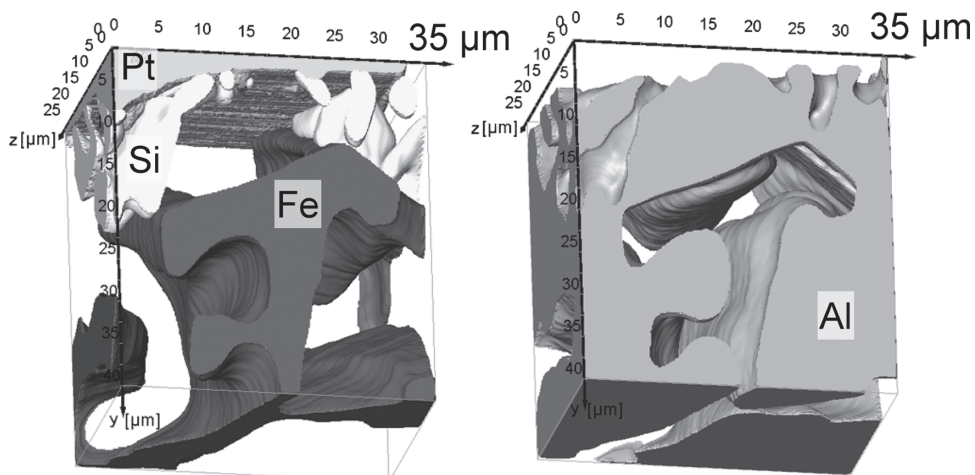


FIGURE 11.13: 3D-reconstruction of FeAl-alloy based on FIB-EDX tomography (adapted from Schaffer et al., 2009).

traceable (Lasagni et al., 2008a). The combination of BSE- and EDX-tomography thus provides important microstructural information at the sub- μm level which cannot otherwise be achieved easily (Engstler et al., 2008). At this stage, the missing piece for complete 3D microstructural characterization of polycrystalline materials was grain orientation contrast.

3.6 3D ELECTRON BACKSCATTER DIFFRACTION (EBSD) BASED ON FIB SERIAL SECTIONING

Electron backscatter diffraction (EBSD) enables the acquisition of crystallographic orientation maps at a maximum resolution of 50 nm. In polycrystalline (but monomineralic) materials, neighboring grains with the same composition cannot be distinguished with BSE- or with EDX-analysis. For such materials the orientation contrast of EBSD opens unique possibilities for the characterization of granular textures. EBSD is particularly well suited for the study of deformation mechanisms such as recrystallization in thermo-mechanical experiments. Since these processes usually result in anisotropic microstructures, 3D microscopy is necessary for a thorough texture analysis. EBSD was therefore also combined with serial sectioning techniques, first with mechanical polishing (Rollett et al., 2007) and later also with FIB-serial sectioning (Konrad et al., 2006; Rowenhorst et al., 2006).

In contrast to the other FIB tomography procedures, EBSD is performed under forward scattering conditions, whereby the angle between surface normal and electron beam directions (incident and scattered beams) is 70°. In order to ensure accessibility of the FIB prepared surface under 70°, a so-called “cantilever beam geometry” was proposed (Groeber et al., 2006; Uchic et al., 2006). As an alternative approach, the block lift-out technique (Schaffer and Wagner, 2008) and other preparation methods (Lasagni et al., 2008b) were developed. During the serial sectioning procedure with the cantilever geometry, the sample is rotated 180° (see Figure 11.6, right) in order to change between the “sectioning position” (in plane with ion beam) and the “EBSD position” (70° between electron beam and normal to FIB prepared surface).

430 APPLICATIONS

Initially, FIB-EBSD serial sectioning was performed manually for the study of the microstructural evolution in warm-rolled Fe₃Al-based alloy (Konrad et al., 2006). Small stacks of about 5 sections were acquired with a z-spacing of 400 nm and the acquisition time was comparatively slow (3 hours per image). It was shown that secondary particles, which are added for mechanical strengthening at elevated temperatures, lead to the formation of strong orientation gradients at the particle-matrix interface. Apparently, the areas with high orientation gradients act as nucleation sites for strain induced recrystallization.

Scripting for serial EBSD acquisition with fully automated sample rotation and repositioning were then introduced, which also allowed the optional combination with ISE-, BSE- and/or EDX-imaging (Groeber et al., 2006; Uchic et al., 2006). The FIB-EBSD tomography was then used in numerous studies such as:

- Quantification of granular textures (grains size, grain orientation, grain surface/perimeter) in Ni-base alloys with γ' -precipitates (Uchic et al., 2006).
- Grain rotation below a conical nanoindentation was described for a (111)Cu single crystal (Zaafarani et al., 2006). Thereby, FIB-EBSD tomography enables insight into the plastic/elastoplastic deformation mechanisms at the crystal lattice level. (Note: in previous investigations with FIB-SEM tomography the deformation patterns could only be investigated at larger scales, e.g., change of layer thickness under nanoindents (Inkson et al., 2001b; Soldera et al., 2007).
- Further FIB-EBSD investigations include microstructural analyses of perlites in carbon steel and fatigue cracks in steel and alloy (Zaefferer et al., 2008; Xu et al., 2007; Motoyashiki et al., 2007).
- 3D characterization of granular textures in thin films with various compositions such as diamond, Ni-Co and Ni-Pt (Liu et al., 2008; Bastos et al., 2008; Jeanvoine et al., 2008; West and Thomson, 2009).
- Last but not least, also polycrystalline ceramic materials were analyzed with 3D-FIB-EBSD (Dillon and Rohrer, 2009).

More detailed descriptions of this specific methodology are presented in recent reviews about FIB-EBSD-tomography (Zaefferer and Wright, 2009) and the corresponding computational processing of 3D-EBSD data (Groeber et al., 2009).

4 CONCLUSIONS: CURRENT STATUS AND NEEDS FOR FURTHER DEVELOPMENTS

FIB tomography is nowadays a versatile method that enables automated acquisition of large image stacks at resolutions below 10 nm. In addition, the ability to perform FIB serial sectioning with different detection modes enables the synchronous acquisition of microstructural (BSE, ISE), chemical (EDX) and crystallographic (EBSD) information from the same sample. These unique 3D-imaging capabilities open new possibilities for 3D microstructural investigations in materials, geo-, environmental, and life sciences. Nevertheless, the current state of FIB serial sectioning suffers from a few, but distinct limitations, which impose the necessity for further improvements:

- Resolution vs. volume: As discussed in the introduction (see also Figure 11.1), the representative analysis of heterogeneous microstructures infers contradicting requirements of a large volume and high magnifications at the same time. FIB tomography is

mainly restricted in the size of the volume due to limitations of ion-milling capabilities. Improvements of the focused ion beam columns should therefore allow faster sputter rates by maintaining the high precision. In this context it is also important to note that alternative techniques for sequential erosion of large areas have been introduced recently, which include broad ion beam (BIB) (Desbois et al., 2009) and mechanical systems (e.g., Micromiller- and RoboMet.3D-systems described by Alkemper and Vorhees, 2001; Spowart et al., 2003). In the near future, intelligent combinations of FIB tomography with BIB or with mechanical polishing techniques may open new possibilities for the analysis of larger volumes at high resolutions.

- Acquisition time and detector sensitivity: FIB serial sectioning is currently strongly limited by relatively long acquisition times. Improved detector sensitivities are therefore required, which enable faster stack acquisition. Recent developments in this field include energy sensitive BSE-detectors for low kV imaging and Silicon-Drift Detectors with wide solid angle for EDX-acquisition with higher acquisition rates. Further improvements of the acquisition rate could enable new “high throughput” applications, such as routine testing of nano-materials and failure analysis.
- Charging and drift: For non-conductive samples, charging of the FIB-milled surface is still a serious problem. Especially for FIB-EDX tomography (which requires high kV and high beam currents) charging of insulating materials induces image distortions and drift. Therefore, in-situ charge neutralization and improved drift-compensation procedures are required.
- 3D-data processing and intelligent automation: Image acquisition and visualization (i.e., “slice and view”) represent only half of the task that has to be solved in order to establish meaningful microstructure-property relationships. Numerous standard software packages for the “off-line” data processing (3D-reconstruction and–visualization) are available. However, suitable software for reliable quantification of complex topological parameters is largely missing (e.g. characterization of skeletonized pore networks or statistical analysis of particle shape and counting of particle-particle contacts). In addition, there are a number of data processing problems that are specific for FIB tomography, especially with regard to analytical FIB-EDX-EBSD tomography. For example, in EDX stacks which were collected at z-step sizes that are smaller than the excitation volume, depth information can be used for spectral deconvolution and improvement of the depth resolution. These new data processing procedures are not yet established.

Furthermore, new possibilities for intelligent automation of multimode FIB serial sectioning can be developed. For example, online “feature recognition” can be used during data acquisition at a coarse and fast serial sectioning. Upon recognition of a specific feature (e.g., failure), the online information can be used to switch to a different serial sectioning mode, e.g., higher magnification or different analytical information (EDX, SIMS, EBSD). In summary, there is much space for further improvements in the fields of intelligent automation of the serial sectioning procedure and for the subsequent quantitative analysis of 3D-microstructures.

REFERENCES

- Alkemper, J., and Vorhees, P. W., 2001. Quantitative serial sectioning analysis. *Journal of Microscopy* 201: 388–394.
 Bansal, R. K., Kubis, A., Hull, R., and Fitz-Gerald, J. M., 2006. High-resolution three-dimensional reconstruction: A combined scanning electron microscope and focused ion-beam approach. *Journal of Vacuum Science and Technology B* 24: 554–561.

432 APPLICATIONS

- Bastos, A., Zaefferer, S., and Raabe, D., 2008. Three dimensional EBSD study on the relationship between triple junctions and columnar grains in electrodeposited Co-Ni films. *Journal of Microscopy* 230: 487–498.
- Boukamp, B., 2006. Anodes sliced with ions. *Nature Materials* 5: 517–518.
- Cantoni, M., 2009. FIB nanotomography: 3D Superstacks, isometric voxels. In S. Abolhassani et al. (eds.), *Interdisciplinary Symposium on 3D Microscopy*. SSOM/PSI, Interlaken, Switzerland, pp. 151.
- Cao, S., Tirry, W., Van Den Broek, W., and Schryvers, D., 2009. Optimization of a FIB/SEM slice-and-view study of the 3D distribution of Ni₄Ti₃ precipitates in Ni-Ti. *Journal of Microscopy* 233: 61–68.
- Crow, G. A., Christman, L., and Utlaut, L., 1995. A focused ion beam secondary ion mass spectroscopy system. *Journal of Vacuum Science and Technology B* 13(6): 2607–2612.
- De Winter, D. A. M., et al., 2009. Tomography of insulating biological and geological materials using focused ion beam (FIB) sectioning and low-kV BSE imaging. *Journal of Microscopy* 233: 372–383.
- Denk, W., and Horstmann, H., 2004. Serial block-face scanning electron microscopy to reconstruct three-dimensional tissue nanostructure. *PLoS Biology* 2: 11.
- Desbois, G., Urai, J. L., Burkhardt, C., Drury, M. R., Hayles, M., and Humbel, B., 2008. Cryogenic vitrification and 3D serial sectioning using high resolution cryo-FIB SEM technology for brine-filled grain boundaries in halite: first results. *Geofluids* 8: 60–72.
- Desbois, G., Urai, J. L. and Kukla, P. A., 2009. Morphology of the pore space in claystones – evidence from BIB/FIB ion beam sectioning and cryo-SEM observations. *eEarth* 4: 15–22.
- Dillon, S. J., and Rohrer, G. S., 2009. Characterization of the grain-boundary character and energy distributions of yttria using automated serial sectioning and EBSD in the FIB. *Journal of the American Ceramic Society* 92: 1580–1585.
- Dunn, D. N., and Hull, R., 1999. Reconstruction of three-dimensional chemistry and geometry using focused ion beam microscopy. *Applied Physics Letters* 75: 3414–3416.
- Elfallagh, F., and Inkson, B. J., 2008. Evolution of residual stress and crack morphologies during 3D FIB tomographic analysis of alumina. *Journal of Microscopy* 230: 240–251.
- Elfallagh, F., and Inkson, B. J., 2009. 3D analysis of crack morphologies in silicate glass using FIB tomography. *Journal of the European Ceramic Society* 29: 47–52.
- Engstler, M., Velichko, A., Klöpper, F., and Mücklich, F., 2008. Automated FIB-EDS-nanotomography and its application to Sr-modified Al-Si foundry alloys. In J. Hirsch, B. Strotzki, and G. Gottstein (eds.), *Aluminium alloys: Their physical and mechanical properties*. Hoboken, NJ: Wiley VCH, pp. 795–800.
- Gostovic, D., Smith, J. R., Kundinger, D. P., Jones, K. S., and Wachsman, E. D., 2007. Three-dimensional reconstruction of porous LSCF cathodes. *Electrochemical and Solid State Letters* 10: B214–B217.
- Gostovic, D., Vito, N. J., O'Hara, K. A., Jones, K. S., and Wachsman, E. D., 2011. Microstructure and connectivity quantification of complex composite solid oxide fuel cell electrode three-dimensional networks. *Journal of the American Ceramic Society* 94: 620–627.
- Groeber, M. A., Haley, B. K., Uchic, M. D., Dimiduk, D. M., and Ghosh, S., 2006. 3D reconstruction and characterization of polycrystalline microstructures using a FIB-SEM system. *Materials Characterization* 57: 259–273.
- Groeber, M. A., Rowenhorst, D. J., and Uchic, M. D., 2009. Collection, processing and analysis of three-dimensional EBSD data sets. In A. J. Schwartz, M. Kumar, B. L. Adams, and D. P. Field (eds.), *Electron backscatter diffraction in materials science*. New York: Springer, pp. 123–138.
- Heymann, J., et al., 2006. Site-specific 3D imaging of cells and tissues with a dual beam microscope. *Journal of Structural Biology* 155: 63–73.
- Heymann, J. A. W., et al., 2009. 3D imaging of mammalian cells with ion-abrasion scanning electron microscopy. *Journal of Structural Biology* 166: 1–7.
- Holzapfel, C., Schäf, W., Marx, M., Vehoff, H., and Mücklich, F., 2007. Interaction of cracks with precipitates and grain boundaries: Understanding crack growth mechanisms through focused ion beam tomography. *Scripta Materialia* 56: 697–700.
- Holzer, L., et al., 2007. Cryo-FIB-nanotomography for quantitative analysis of particle structures in cement suspensions. *Journal of Microscopy* 227: 216–228.

- Holzer, L., Gasser, P., and Münch, B., 2006a. Quantification of capillary pores and hadley grains in cement paste using FIB-nanotomography. In M.S. Konsta-Gdoutos (ed.), *Measuring, monitoring and modeling concrete properties*. Dordrecht: Springer, pp. 509–516.
- Holzer, L., Indutnyi, F., Gasser, P., Münch, B., and Wegmann, M., 2004. 3D analysis of porous BaTiO₃ ceramics using FIB nanotomography. *Journal of Microscopy* 216(1): 84–95.
- Holzer, L., Iwanschitz, B., Hocker, Th., Prestat, M., Wiedenmann, D., Vogt, U., Holtappels, P., Sfeir, J., Mai, A., and Graule, Th., 20011. Microstructure degradation of cermet anodes for solid oxide fuel cells: Quantification of nickel grain growth in dry and in humid atmospheres. *Journal of Power Sources* 196: 1279–1294.
- Holzer, L., Muench, B., Leemann, A., and Gasser, P., 2006b. Quantification of capillary porosity in cement paste using high resolution 3D-microscopy: Potential and limitations of FIB-nanotomography. In J. Marchand, B. Bissonnette, R. Gagne, M. Jolin, and F. Paradis (eds.), *Advances in concrete*. Quebec: RILEM, pp. 247 (electronic media).
- Holzer, L., Muench, B., Rizzi, M., Wepf, R., and Marschall, P., 2010. 3D-microstructure analysis of hydrated bentonite with cryo-stabilized pore water. *Applied Clay Science*: 45: 330–342.
- Holzer, L., and Münch, B., 2009. Towards reproducible three-dimensional microstructure analysis of granular materials and complex suspensions. *Microscopy and Microanalysis* 15: 130–146.
- Holzer, L., Münch, B., Wegmann, M., Flatt, R., and Gasser, P., 2006c. FIB-nanotomography of particulate systems – Part I: particle shape and topology of interfaces. *Journal of the American Ceramic Society* 89: 2577–2585.
- Hutter, H., and Grasserbauer, M., 1992. Three dimensional ultra trace analysis of materials. *Mikrochimica Acta* 107: 137–148.
- Inkson, B. J., Mulvihill, M., and Möbus, G., 2001a. 3D determination of grain shape in a FeAl-based nanocomposite by 3D FIB tomography. *Scripta Materialia* 45: 753–758.
- Inkson, B. J., Olsen, S., Norris, D. J., O'Neill, A. G., and Möbus, G., 2003. 3D determination of a MOSFET gate morphology by FIB tomography. *Microsc. Semicond. Mater. Conf. Inst. Phys. Conf.*, Cambridge, pp. 611–616.
- Inkson, B. J., Steer, T., Möbus, G., and Wagner, T., 2001b. Subsurface nanoindentation deformation of Cu-Al multilayers mapped in 3D by focused ion beam microscopy. *Journal of Microscopy* 201: 256–269.
- Izzo, J. R., et al., 2008. Nondestructive reconstruction and analysis of SOFC anodes using x-ray computed tomography at sub-50 nm resolution. *Journal of the Electrochemical Society* 155: B504–508.
- Jeanvoine, N., Holzapfel, C., Soldera, F. and Mücklich, F., 2006. 3D investigations of plasma erosion craters using FIB/SEM Dual Beam techniques. *Practical Metallography* 43: 470–482.
- Jeanvoine, N., Holzapfel, C., Soldera, F. and Mücklich, F., 2008. Microstructure characterization of electrical discharge craters using FIB/SEM dual beam techniques. *Advanced Engineering Materials* 10: 973–977.
- Knott, G., Marchman, H., Wall, D., and Lich, B., 2008. Serial section scanning electron microscopy of adult brain tissue using focused ion beam milling. *Journal of Neuroscience* 28: 2959–2964.
- Konrad, J., Zaefferer, S., and Raabe, D., 2006. Investigation of orientation gradients around a hard Laves particle in a warm-rolled Fe3Al-based alloy using a 3D EBSD-FIB technique. *Acta Materialia* 54: 1369–1380.
- Kotula, P. G., Keenan, M. R., and Michael, J. R., 2003. Automated analysis of SEM X-ray spectral images. *Microscopy and Microanalysis* 9: 1–17.
- Kotula, P. G., Keenan, M. R., and Michael, J. R., 2006. Tomographic spectral imaging with multivariate statistical analysis: Comprehensive 3d microanalysis. *Microscopy and Microanalysis* 12: 36–48.
- Kubis, A. J., Shiflet, G. J., Dunn, D. N., and Hull, R., 2004. Focused ion-beam tomography. *Metallurgical and Materials Transactions A*, 35A: 1935–1943.
- Lasagni, F., Lasagni, A., Engstler, M., Degischer, H. P., and Mücklich, F., 2008a. Nano-characterization of cast structures by FIB-tomography. *Advanced Engineering Materials* 10: 62–66.
- Lasagni, F., Lasagni, A., Holzapfel, C., and Mücklich, F., 2008b. Sample preparation of Al-alloys for 3D FIB nano-characterization. *Practical Metallography* 45: 246–250.

434 APPLICATIONS

- Lasagni, F., Lasagni, A., Holzapfel, C., Mücklich, F. and Degischer, H. P., 2006. Three-dimensional characterization of unmodified and Sr-modified Al-Si eutectics by FIB and FIB EDX tomography. *Advanced Engineering Materials* 8: 719–723.
- Lasagni, F., et al., 2007. Three dimensional characterization of “as-cast” and solution-treated AlSi12(Sr) alloys by high-resolution FIB tomography. *Acta Materialia* 55: 3875–3882.
- Liu, T., Raabe, D., and Zaefferer, S., 2008. A 3D tomographic EBSD analysis of a CVD diamond thin film. *Sci. Technol. Adv. Mater.* 9: 035013.
- Martys, N. S., 2005. Study of a dissipative particle dynamics based approach for modelling suspensions. *Journal of Rheology* 49: 401–424.
- McGrath, D., and Munroe, P. R., 2007. Imaging and analysis of 3-D structure using a dual beam FIB. *Microscopy Research and Technique* 70: 186–194.
- McLachlan, D. S., Blaszkiewicz, M., and Newnham, R., 1990. Electrical resistivity of composites. *Journal of the American Ceramic Society* 73: 2187–2203.
- Mimura, R., Takayama, H., and Takai, M., 2003. Nanometer resolution three-dimensional microprobe RBS analyses by using a 200 kV focused ion beam system. *Nuclear Instruments and Methods in Physics Research*, B210: 104–107.
- Mobus, G., and Inkson, B. J., 2007. Nanoscale tomography in materials science. *Materials Today* 10: 18–25.
- Motoyashiki, Y., Bruckner-Foit, A., and Sugita, A., 2007. Investigation of small crack behaviour under cyclic loading in a dual phase steel with an FIB tomography technique. *Fatigue & Fracture of Engineering Materials & Structures* 30: 556–564.
- Münch, B., Gasser, P., Flatt, R., and Holzer, L., 2006a. FIB-nanotomography of particulate systems – Part II: Particle recognition and effect of boundary truncation. *Journal of the American Ceramic Society* 89: 2586–2595.
- Münch, B., Gasser, P., and Holzer, L., 2006b. Simulation of drying shrinkage based on high-resolution 3D pore structure analysis of cement paste. In J. Marchand (ed.), *International Symposium on Advances in Concrete Through Science and Engineering*. RILEM, Quebec, CRIB.
- Münch, B., and Holzer, L., 2008. Contradicting geometrical concepts in pore size analysis attained with electron microscopy and mercury intrusion. *Journal of the American Ceramic Society* 91: 4059–4067.
- Patkin, A. J., and Morrison, G. H., 1982. Secondary ion mass spectrometric image depth profiling for three-dimensional elemental analysis. *Analytical Chemistry* 54: 2–5.
- Rollett, A. D., Lee, S. B., Campman, R., and Rohrer, G. S., 2007. Three-dimensional characterization of microstructure by electron backscatter diffraction. *Annu. Rev. Mater. Res.* 37: 627–658.
- Rowenhorst, D. J., Gupta, A., Feng, C. R. and Spanos, G., 2006. 3D crystallographic and morphological analysis of coarse martensite: Combining EBSD and serial sectioning. *Scripta Materialia* 55: 11–16.
- Russ, J. C., 1999. *The image processing handbook*. Boca Raton, FL: CRC Press.
- Sakamoto, T., Cheng, Z., Takahashi, M., Owari, M., and Nihei, Y., 1998. Development of an Ion and Electron Dual Focused Beam Apparatus for three Dimensional Microanalysis. *Japanese Journal of Applied Physics* 37: 2051–2056.
- Schaffer, M., and Wagner, J., 2008. Block lift-out preparation for 3D experiments in a dual beam focused ion beam microscope. *Microchimica Acta* 161: 421–425.
- Schaffer, M., Wagner, J. and Grogger, W., 2009. 3D-energy-dispersive X-ray spectrometry in a dual-beam FIB (3D-FIB EDXS). In S. Abolhassani et al. (eds.), *Interdisciplinary Symposium on 3D Microscopy*, SSOM/PSI, Interlaken, Switzerland, pp. 43–44.
- Schaffer, M., Wagner, J., Schaffer, B., Schmied, M., and Mulders, H., 2007. Automated three-dimensional X-ray analysis using a dual-beam FIB. *Ultramicroscopy*, 107: 587–597.
- Schroeder-Reiter, E., Pérez-Willard, F., Zeile, U., and Wanner, G., 2009. Focused ion beam (FIB) combined with high resolution scanning electron microscopy: A promising tool for 3D analysis of chromosome architecture. *Journal of Structural Biology* 165: 97–106.
- Smith, J. R., et al., 2009. Evaluation of the relationship between cathode microstructure and electrochemical behavior for SOFCs. *Solid State Ionics* 180: 90–98.
- Soldner, F., Gaillard, Y., Anglada Gomila, M., and Mücklich, F., 2007. FIB-tomography of nanoindentation cracks in zirconia polycrystals. *Microscopy and Microanalysis* 13: 1510–1511.
- Sotah, H., Owari, M., and Nihei, Y., 1991. Three-dimensional analysis of a microstructure by submicron secondary ion mass spectrometry. *Journal of Vacuum Science and Technology B9*: 2638–2640.

- Spowart, J. E., Mullins, H. M., and Puchala, B. T., 2003. Collecting and analyzing microstructures in three dimensions: A fully automated approach. *JOM* 55: 35–37.
- Tanaka, Y., et al., 2003. Development of a chemically assisted micro-beam etching system for three-dimensional microanalysis. *Applied Surface Science* 203: 205–208.
- Tomiyasu, B., Fukuju, I., Komatsubara, H., Owari, M., and Nihei, Y., 1998. High spatial resolution 3D analysis of materials using gallium focused ion beam secondary ion mass spectrometry (FIB SIMS). *Nuclear Instruments and Methods in Physics Research B* 136–138: 1028–1033.
- Trtik, P., Dual, J., Muench, B., and Holzer, L., 2008. Limitation in obtainable surface roughness of hardened cement paste: “virtual” topographic experiment based on focussed ion beam nanotomography datasets. *Journal of Microscopy* 232: 200–206.
- Uchic, M. D., Groeber, M. A., Dimiduk, D. M., and Simmons, J. P., 2006. 3D microstructural characterization of nickel superalloys via serial-sectioning using a dual beam FIB-SEM. *Scripta Materialia* 55: 23–28.
- Uchic, M. D., Holzer, L., Inkson, B. J., Principe, E. L., and Munroe, P., 2007. Three-dimensional microstructural characterization using focused ion beam tomography. *MRS Bulletin* 32: 408–416.
- Velichko, A., Holzapfel, C., Siefers, A., Schladitz, K., and Mücklich, F., 2008. Unambiguous classification of complex microstructures by their three-dimensional parameters applied to graphite in cast iron. *Acta Materialia* 56: 1981–1990.
- West, G. D., and Thomson, R. C., 2009. Combined EBSD/EDS tomography in a dual-beam FIB/FEG-SEM. *Journal of Microscopy* 233: 442–450.
- Wilson, J. R., et al., 2009a. Quantitative three-dimensional microstructure of a solid oxide fuel cell cathode. *Electrochemistry Communications* 11: 1052–1056.
- Wilson, J. R., et al., 2009b. Three-dimensional analysis of solid oxide fuel cell Ni-YSZ anode interconnectivity. *Microscopy and Microanalysis* 15: 71–77.
- Wilson, J. R., et al., 2006. Three-dimensional reconstruction of a solid-oxide fuel-cell anode. *Nature Materials* 5: 541–544.
- Wu, H. Z., Roberts, S. G., Möbus, G., and Inkson, B. J., 2003. Subsurface damage analysis by TEM and 3D FIB crack mapping in alumina and alumina/5vol%SiC nanocomposites. *Acta Materialia* 51: 149–163.
- Xu, W., Ferry, M., Mateescu, N., Cairney, J. M., and Humphreys, F. J., 2007. Techniques for generating 3-D EBSD microstructures by FIB tomography. *Materials Characterization* 58: 961–967.
- Zaafarani, N., Raabe, D., Singh, R. N., Roters, F., and Zaefferer, S., 2006. Three-dimensional investigation of the texture and microstructure below a nanoindent in a Cu single crystal using 3D EBSD and crystal plasticity finite element simulations. *Acta Materialia* 54: 1863–1876.
- Zaefferer, S., and Wright, S. I., 2009. Three-dimensional orientation microscopy by serial sectioning and EBSD-based orientation mapping in a FIB-SEM. In A. J. Schwartz, M. Kumar, B. L. Adams, and D. P. Filed (eds.), *Electron backscatter diffraction in materials science*. New York: Springer, pp. 109–122.
- Zaefferer, S., Wright, S. I., and Raabe, D., 2008. Three-dimensional orientation microscopy in a focused ion beam-scanning electron microscope: A new dimension of microstructure characterization. *Metallurgical and Materials Transactions A*, 39A: 374–389.
- Zingg, A. et al., 2008. The microstructure of dispersed and non-dispersed fresh cement pastes – New insight by cryo-microscopy. *Cement and Concrete Research* 38: 522–529.